Evidence for an active, transcrustal magma system in the last 60 ka and eruptive degassing budget (H2O, CO2, S, F, Cl, Br): The case of Dominica

Thiebaut d'Augustin, Hélène Balcone-Boissard, Georges Boudon, Caroline Martel, Etienne Deloule, Pierre Burckel

Correspondence to:
T. d'Augustin,
thiebaut.daugustin@sorbonne-univer-site.fr

Evidence for an Active, Transcrustal Magma System in the Last 60 ka and Eruptive Degassing Budget (H2O, CO2, S, F, Cl, Br): The Case of Dominica

T. d'Augustin[1], H. Balcone-Boissard[1], G. Boudon[2], C. Martel[3], E. Deloule[4], and P. Bürckel[2]

[1]Institut des Sciences de la Terre de Paris (ISTeP), UMR 7193, CNRS-Sorbonne Université, Paris, France, [2]Institut de Physique du Globe de Paris (IPGP), CNRS, Université de Paris, Paris, France, [3]Institut des Sciences de la Terre d'Orléans (ISTO), UMR 7327, Université d'Orléans-CNRS/INSU-BRGM, Orléans, France, [4]CRPG, UMR 5873, CNRS-Université de Lorraine, Vandœuvre-lès-Nancy, France

Abstract The Morne Trois Pitons-Micotrin volcanic complex on the island of Dominica (Lesser Antilles) emitted a series of plinian eruptions between 18 and 9 ka BP. We studied it to constrain magma storage conditions and volatile degassing balances, by comparison with the three previous ignimbrites (~60–24 ka BP). Volatile concentrations in glass inclusions and mineral-melt thermobarometry indicate storage at ≤ 200 MPa (~6–8 km) and 860–880°C. The magmas feeding these plinian eruptions were stored at a shallower depth than those that older ignimbrites from the same volcanic complex and stored at ~16 km. Close magma composition and similar halogen ratios, however, suggest a common source for the magmas feeding both the plinian eruptions and the ignimbrites. The large eruptive fluxes of F, Cl, and Br to the atmosphere (up to 1.4–2.8×10^{-1} Mt/km^3, 1.5–4.0 Mt/km^3, and 2–4×10^{-2} Mt/km^3, respectively), estimated by the petrological method, support the potentially important role of volcanic halogens in modifying the chemistry of the atmosphere, though Cl is underestimated here because of buffering in a fluid phase. The behavior of S, potentially partitioned in the same fluid phase, prevents here the calculation of an eruptive outgassing budget.

1. Introduction

Volcanoes pose significant hazards for humans and the environment (e.g., Fearnley et al., 2018; Robock, 2015). Volcanic gas emissions of highly reactive species such as sulfur and halogens (F, Cl, Br) species have crucial long-term consequences on stratosphere composition and thus on Earth's climate (Schmidt & Robock, 2015). It is therefore important to constrain volcanic gas fluxes before reactions in the plume disturb measurements to understand their role on the atmosphere chemistry. Volcanic halogen contributions to the atmosphere during past eruptions remain poorly understood (e.g., Mather, 2015), and long-term volcanic impact of halogens on the atmosphere may be largely underestimated. The degassing budgets of magma systems depend on the absolute abundance and the solubility of their volatile species (Balcone-Boissard et al., 2010; Harms & Schmincke, 2000). To fully quantify volatile behavior and to establish the degassing budget of magma systems or individual eruptions, it is necessary to study magma volatile composition and concentrations from crustal reservoirs up to eruption.

The first classical model of a magma storage zone within the crust was a more or less spherical "pocket" of liquid material within the solid crust, that is, a tank-like "magma chamber." However, current models advocate that most crustal-scale magma plumbing system are made up of "crystal-rich magma mush" (Bachmann & Bergantz, 2008; Cashman et al., 2017; Cooper, 2017). Most of this mush is too viscous to flow, but magma can be mobilized by several processes. The magma is generally thought to be stored at different levels, with the most eruptible portions in the upper part of the reservoirs (Bachmann & Bergantz, 2008; Miller & Wark, 2008), which only represent a low fraction of the total magma volume (Annen et al., 2008). These storage areas, located at variable depths within the crustal column, are inferred to communicate through a fracture network, forming a transcrustal magmatic system (Cashman et al., 2017; Sparks & Cashman, 2017).

The study of volatile elements in magmatic systems moreover provides valuable information on storage conditions as their solubility depends upon physical and chemical conditions in the reservoirs (e.g., Carroll, 2005;

Clemente, 2004; Di Matteo et al., 2004; Ghiorso & Gualda, 2015; Newman & Lowenstern, 2002; Papale, 1997; Putirka, 2008). Melt inclusions are small pockets of quenched magma enclosed in crystals, which are compositional recorders of the magma that surrounded the crystal when they were trapped. Their volatile content is representative of pre-eruptive conditions, unless the inclusions have undergone post-entrapment modifications (Kent, 2008; Métrich & Wallace, 2008). The melt inclusion compositions can thus be used to determine magma storage conditions (Ghiorso & Gualda, 2015; Putirka, 2008; Wallace et al., 2015) and also to establish degassing budgets by comparison with residual volatile contents measured in matrix glasses. This approach, also called the "petrological method," may provide tight constraints on volatile degassing prior to chemical reactions within volcanic emission plumes (Aiuppa, 2009; Roberts et al., 2009).

Our study quantifies the volatile degassing budget during the explosive eruptions produced by Morne Trois Pitons-Micotrin (MTPM) volcanic complex during the last 18 ka and also provides new constraints on the magma plumbing system beneath the central part of Dominica. We have focused our study on a series of plinian eruptions that occurred over the last 20 ka following a series of more voluminous ignimbrites dated to 60–20 ka that have already studied (Balcone-Boissard et al., 2018; Boudon et al., 2017; Solaro et al., 2019). We conclude by comparing our insights on the magma plumbing system beneath Dominica to other volcanic systems of the Lesser Antilles arc and by comparing halogen and S degassing budgets to those of major explosive eruptions that have occurred worldwide.

2. Geological Context

The Lesser Antilles arc is an 800 km long subduction arc, which extends from Anguilla and Saba island (in the North) to Grenada island (in the South), with a convexity toward the east (Figure 1a). The arc is active since the late Miocene, resulting from subduction of the North-American plate beneath the Caribbean plate at low velocity (~2 cm/year) (Macdonald et al., 2000) that yields a low magma production rate (5 km^3/Ma/km) (Wadge, 1984). North of Dominica, the arc is divided into two segments. The outer segment, from Anguilla to Dominica, is made up of old volcanic islands, which are mostly covered by carbonate platforms. The inner segment, from Saba island to Dominica, comprises the youngest islands with active volcanoes (Mount Scenery [Saba], Mount Liamuiga [St Kitts], Soufriere Hills [Montserrat], and Soufrière [Guadeloupe]). South of Dominica, the two segments of the arc merge, where recent volcanism builds on old volcanic islands.

Dominica is located in the central part of the arc, where the two northern segments merge. In contrast to the other islands of the arc that have only one active volcano, Dominica has four main active volcanic centers. These are, from North to South, Morne aux Diables, where a seismic crisis occurred in 2010 (Watts et al., 2012), Morne Diablotins, MTPM, and Plat Pays Volcanic Complex (PPVC). Small satellite centers are also present south of MTPM.

Numerous studies have characterized Dominica's volcanic activity (Lindsay, Smith, et al., 2005; Smith et al., 2013). Sigurdsson (1972), Sparks et al. (1980), and Whitham (1989) specifically studied some large ignimbrites and their offshore extension. Other studies focused on the volcanic evolution of the southern PPVC complex and its magmatic evolution (Gurenko et al., 2005; Halama et al., 2006; Le Friant et al., 2002; Lindsay et al., 2003; Lindsay, Trumbull, et al., 2005; Roobol et al., 1983). More recently, Smith et al. (2013), Howe et al. (2015, 2014), and Boudon et al. (2017) proposed a stratigraphy of the explosive eruptions that occurred in the central part of Dominica. Howe et al. (2014) and Frey et al. (2018) dated ignimbrites by U-Th/He and U-Th zircon ages, respectively, whereas Boudon et al. (2017) proposed a detailed chronostratigraphy based on a series of ^{14}C dates. The storage conditions of the magma at the origin of the large ignimbrites from the central part of Dominica have been determined on the basis of volatile contents preserved in melt inclusions (Balcone-Boissard et al., 2018) and through phase-equilibrium experiments (Solaro et al., 2019).

Boudon et al. (2017) distinguished five large ignimbrites of 3 to 5 km^3 (DRE). Two of the corresponding eruptions were discharged from Morne Diablotins volcano (Grande Savane and Layou; Layou being dated at 50.6 ka, Figure 1c). The other three ignimbrites were generated by the MTPM volcano: the Grand Bay (>60 ka) Roseau (33 ka) and Grand Fond (24 ka) ignimbrites. The five eruptions each started with a plinian phase followed by voluminous pumiceous pyroclastic density currents (PDCs) that filled several valleys and flowed into the sea generating thick turbidity currents. On-land, the PDC deposits are up to several tens of meters thick and welded (Boudon et al., 2017). The MTPM volcano also produced a series of plinian eruptions, which generated pumice fallout deposits and few PDCs (Boudon et al., 2017) (Figures 1b and 1c).
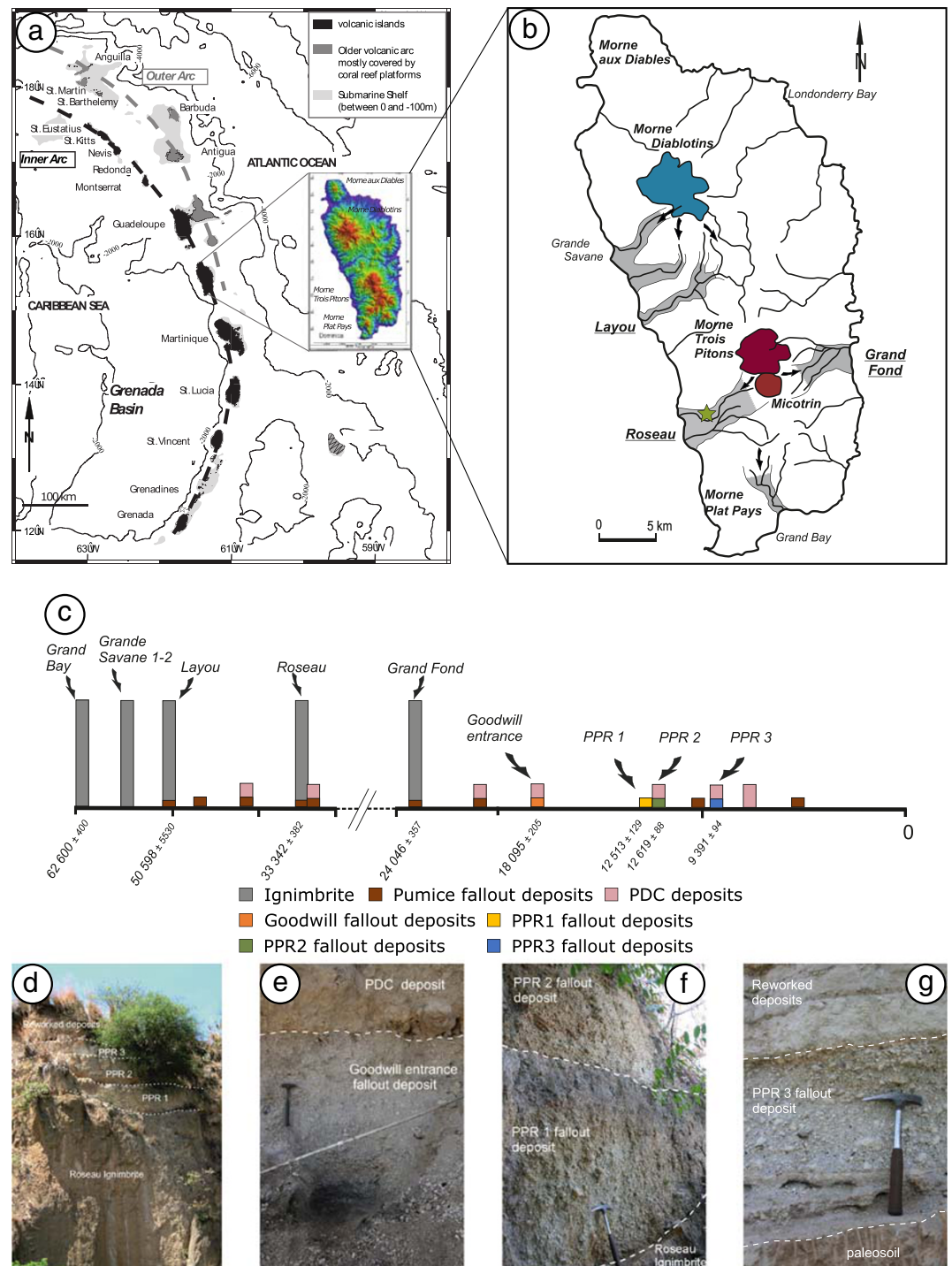
Figure 1. (a) Map of the Lesser Antilles arc and Dominica island. (b) Map of Dominica with Morne Diablotins volcanic system (blue), Morne Trois Pitons-Micotrin volcanic system (red), and ignimbrite deposits (gray). The green star indicates the sampling location. (c) Chronology of the plinian eruptions of the central part of Dominica (Morne Diablotins and Morne Trois Pitons-Micotrin) for the last 60 ka (modified from Boudon et al., 2017). Gray: large ignimbrite deposits; orange, yellow, green, and blue: pumice fallout deposits from Goodwill, PPR1, PPR2, and PPR3, respectively; brown: pumice fallout deposits from other plinian eruptions; and pink: PDC deposits from Plinian eruptions. (d) Photos of the pumiceous deposits in the Goodwill quarry (Roseau) showing fallout deposits from three plinian eruptions (PPR1, PPR2, and PPR3) overlying the Roseau ignimbritic deposit. (e) Goodwill entrance fallout deposit. (f) PPR1 and PPR2 fallout deposits. (g) PPR3 fallout deposit.

The volume of fall deposits from the plinian eruptions are 1 order of magnitude lower than the volume of ignimbrite deposits (0.3 to 0.5 and 3 to 5 km^3, respectively, Boudon et al., 2017). Our work focuses on four of the post-ignimbrite plinian eruptions: "Goodwill entrance" (18 ka; hereafter referred as Goodwill) and "Plinian Post-Roseau" (PPR) 1 to 3 (12.6, 12.5, and 9.4 ka, respectively). The deposits of these four plinian eruptions are found on the western coast in the Roseau valley. The Goodwill eruption produced a plinian fall deposit (Figure 1e) overlain by a PDC deposit. These deposits are confined to a valley within the Roseau ignimbritic deposits. The reference section is located near the Goodwill quarry (15°18′30″N, 61°23′03″W; Boudon et al., 2017). The PPR1 to PPR3 deposits cover the Roseau ignimbrites in the Goodwill quarry (Figures 1d and 1f). PPR1 is a normally graded plinian deposit (1.25 m thick; Figure 1f); no PDC deposits are recognized to be associated with this eruption. PPR2 and PPR3 are plinian eruptions, both associated with PDCs recognized on field (Figures 1d, 1f, and 1g). At the top of the Goodwill quarry, thick reworked deposits cover the PPR3 pumice fallout deposits (Figure 1d).

3. Materials and Methods

3.1. Sampling

Pumice fallout deposits were studied for each of the four eruptions (Figure 1). Pumice samples were collected between 2011 and 2013 as part of large sampling campaigns (Boudon et al., 2017). Due to thick vegetation, sampling was only possible only along sea cliffs, in large valleys, and on roadsides. Sampling location is located on Figure 1b by a green star (see also Figure 2b of Boudon et al., 2017).

3.2. Sample Preparation

Several unaltered pumices from each eruption were collected. The pumices were gently crushed together to coarse powders (up to 3 mm) to avoid breaking crystals. The powder was divided into two identical parts. One part was further crushed into fine powder for whole rock analysis; the other part was used to separate glassy matrix and minerals by sieving into different size fractions (125–250 μm; 250–355 μm; 355–500 μm; 500–710 μm; and 710 μm to 1 mm). Each size fraction was first washed in an ultrasonic bath to separate fine particles, and minerals were then separated by density in water.

Euhedral crystals were most abundant in the 355–500 μm size fractions. Orthopyroxene, clinopyroxene, plagioclase, and magnetite (hereafter referred as OPX, CPX, PLAG, and MGT, respectively) were handpicked under a binocular microscope, mounted separately in epoxy resin. The mounts were roughly polished using sandpaper with decreasing grain size and finally polished using 0.3 μm using Al$_2$O$_3$-impregnated lapping films, to expose melt inclusions at the surface (Supporting Information Figures S1–S3). Some pumice fragments were also mounted in epoxy resin and polished for point analysis of residual glass.

3.3. Textural Observations and Geochemical Measurements

Textural observations were performed with a scanning electron microscope (SEM) at the "Institut des Sciences de la Terre de Paris," Sorbonne Université (Paris). The minerals, which are translucent under an optical microscope (with the exception of MGT), allow the shrinkage bubbles to be perceived. After having selected the melt inclusions that do not contain any, we first screened them using energy-dispersive X-ray spectroscopy (EDS) to determine their composition, to avoid analyzing crystallized or partly crystallized inclusions during subsequent analysis (Figures S1–S3). Glass shards mounted in epoxy were also screened by SEM in order to select matrix glass area large enough to be analyzed by electron microprobe.

Point analyses of major elements (Si, Ti, Al, Fe, Mg, Mn, Ca, Na, K, P), F, and Cl were performed on selected melt inclusions, host minerals, and residual glasses using a CAMECA SX five electron microprobe (EPMA) at Camparis (Paris). An acceleration voltage of 15 keV was used, with a beam current of 10 nA for major elements and of 80 nA for F and Cl. Counting time was 10 s for major elements, 120 s for F, and 60 s for Cl and S, to provide lower detection limits. Na was analyzed first to minimize loss by volatilization under the electron beam. The beam size was also defocused to 10 μm to minimize volatile loss for all glass analyses, while it was focused for host mineral analyses. For inter-calibration of EPMA sessions, three internal standards were analyzed in the same conditions as the samples (CO5, LIP, and LGM, Balcone-Boissard et al., 2008). Standards and samples were carbon-coated together to avoid bias caused by a different coat thickness.

H_2O, CO_2, Br, and S concentrations in melt inclusions were measured at the Centre de Recherches Pétrographiques et Géochimiques (CRPG) of Nancy (France), using a IMS 1280 HR2 Secondary Ion Mass Spectrometer (SIMS) following the methodology of Bouvier et al. (2010), Métrich and Deloule (2014) (for H_2O, CO_2, and S), and Cadoux et al. (2017) (for Br). Calibration curves for H_2O, CO_2, S, and Br were calculated using best fit regressions in $[H_2O]$ versus $^{16}OH/^{18}O$, $[CO_2]$ versus $^{12}C/^{18}O$, $[S]$ versus $^{32}S/^{16}O$, and $[Br]/[SiO_2]$ versus $^{81}Br/^{29}SI^{16}O_3$, respectively, from standards coming from Jochum et al. (2006). H_2O, and CO_2 and S calibration curves (Figure S4) were normalized to oxygen because the oxygen content is approximately constant in all magma compositions from basalts to rhyolites, regardless the silica content. The signal is thus less composition dependent than if it was normalized to silica. Moreover, OH^- ions are formed in the plasma, which make their concentration independent from the silica content. Br calibration curve was normalized to silica content in the inclusion (previously measured with EPMA) to cast off silica content dependency. Regression curve for H_2O was fitted by a polynomial, whereas CO_2, S, and Br were fitted by a linear regression. For each volatile species, sample concentration fell within standard composition range. The mean standard deviation on H_2O measurements is 125 ppm, 43 ppm for carbon dioxide, and 1 ppm for sulfur. We monitored signal stability during the analysis of every volatile element, which allowed us to rule out inclusions where the signal was unstable.

Trace element concentrations in melt inclusions (measured as ^6Li, ^7Li, ^{27}Al, ^{43}Ca, ^{44}Ca, ^{59}Co, ^{60}Ni, ^{85}Rb, ^{88}Sr, ^{89}Y, ^{90}Zr, ^{93}Nb, ^{137}Ba, ^{139}La, ^{140}Ce, ^{141}Pr, ^{146}Nd, ^{147}Sm, ^{153}Eu, ^{157}Gd, ^{159}Tb, ^{163}Dy, ^{165}Ho, ^{166}Er, ^{169}Tm, ^{172}Yb, ^{175}Lu, ^{232}Th, ^{238}U) were analyzed by laser-ablation ICP-MS (using an ArF RESOlution excimer laser-ablation system coupled to a high-resolution sector field Thermo Finnigan Element XR mass spectrometer) at the Laboratoire Magmas et Volcans of Clermont-Ferrand, with the following conditions: Ablation gasses were pure He (730 ml/min) and N_2 (5.5 ml/min) with Ar as auxiliary and cooling gas; laser diameter was varied between 9 μm for the smallest inclusions and 30 μm for the largest; fluence was set to 2.8 J·cm^{-2}; and measurements were divided into background acquisition (30 s) and peak acquisition (90 s). All analyses were performed in low-resolution mode. NIST612 was used as external (primary) standard (Gagnon et al., 2008), while NIST610 and BCR-2G were used as quality controls (Gagnon et al., 2008; Sigmarsson et al., 2013). ^{44}Ca was used as the internal standard, which was determined by electron microprobe. Primary standards were analyzed three times at the beginning and at the end of each run between 10 and 15 sample and control analyses.

Whole-rock major-element compositions reported are those determined by Boudon et al. (2017), which were analyzed by ICP-OES at CRPG (Carignan et al., 2001). Bulk halogen and S contents were extracted by pyrohydrolysis and analyzed by ionic chromatography for F, Cl, and SO_4^{2-} and by ICP-MS for Br at IPGP (Balcone-Boissard et al., 2009; Michel & Villemant, 2003).

4. Results

4.1. Post-Entrapment Modifications of Melt Inclusions

Melt inclusions give valuable information on magma storage conditions, provided that they stay unmodified after entrapment. Many authors cautioned against melt inclusions changes after entrapment, such as crystallization of daughter minerals, H^+ diffusion through the host mineral, or CO_2 migration into shrinkage bubbles (e.g., Baker, 2008; Cannatelli et al., 2016; Danyushevsky et al., 2002; Kent, 2008; Métrich & Wallace, 2008; Sobolev, 1996; Sobolev & Danyushevsky, 1994), so it is important to ensure that the composition of the inclusions has not been altered. We have therefore paid particular attention to analyze only bubble-free melt inclusions. Obviously recrystallized melt inclusions (i.e., microlite-bearing ones) were also avoided; after measurements, we determined the degree of recrystallization, based on Fe-Mg or Ca-Na partition coefficients (K_D) proposed by Putirka (2008). The Rhodes diagrams on Figure S5 show the difference between each melt inclusion and the equilibrium. The results suggest <3% recrystallization of melt inclusions in OPX and CPX. Melt inclusions in PLAG appear to have experienced recrystallization by typically ~5%, but sometimes up to 10%. Only melt inclusion compositions with recrystallization limited to <8% were considered.

Just as we only selected bubble-free inclusions and checked the signal stability, we made sure that analysis gave consistent results and rejected outliers. CO_2 is poorly affected by diffusion through the host mineral but
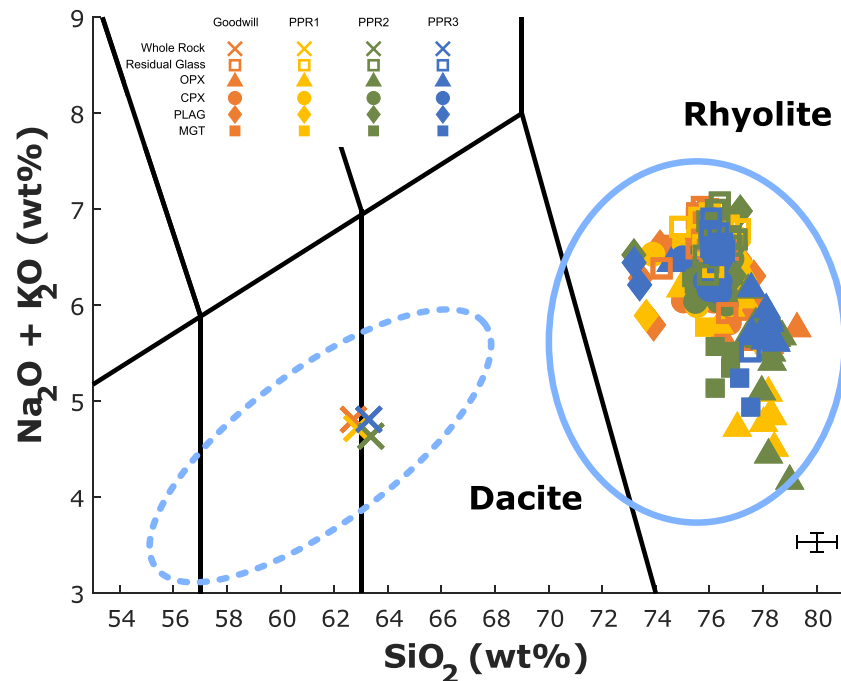
Figure 2. TAS diagram for whole rocks (crosses), residual glasses (empty squares), and selected melt inclusions hosted by OPX (filled triangles), CPX (filled circles), PLAG (filled diamonds), and MGT (filled squares), presented for Goodwill (orange), PPR1 (yellow), PPR2 (green), and PPR3 (blue). The solid blue circle and the dashed blue circle mark domains of ignimbrite melt inclusion and whole rocks compositions, respectively (from Balcone-Boissard et al., 2018).

much more by the formation of shrinkage bubbles (Métrich & Wallace, 2008; Portnyagin et al., 2008). However, two incompatible and volatile species such as CO_2 and H_2O should have the same behavior whereas high and low CO_2 values were associated to mean H_2O concentrations over the range of values. It is therefore unlikely that the measurements were impacted by shrinkage bubbles. Regarding H^+ diffusion through the host mineral, as also observed on Dominica (Gurenko et al., 2005), losses of both H^+ and Li resulted in low concentrations of both hydrogen and Li and were higher in PLAG than in OPX, with diffusion in the latter being slower. Conversely, we observe that the lowest Li values are measured in CPX inclusions and correspond to high water contents (Figure S6). Thus, the values seem only slightly affected by H^+ loss.

4.2. Melt Inclusion and Matrix Glass Major-Element Composition

The whole rocks of the four studied eruptions have a homogeneous major-element composition and lie at and near the boundary between the andesite and the dacite field in the TAS diagram (Boudon et al., 2017; Figure 2 and Table S1). A total of 197 melt inclusions was analyzed for the four studied eruptions, which were enclosed in OPX, CPX, PLAG, and MGT. After elimination of melt inclusions with too high PEC, 171 melt inclusions were retained. Their compositions are listed in supporting information (Tables S2 and S4). The number of melt inclusions analyzed within each mineral species is not representative of the abundance of the minerals in the magma, as the size and quantity of melt inclusions drastically vary from one mineral to another. In OPX, melt inclusions are abundant, reaching 90 μm in maximum dimension. In PLAG and CPX, melt inclusions are also abundant, and they are commonly 20 to 40 μm wide, but they often contain bubbles or microcrystals. Melt inclusions in MGT, in contrast, are rare, they are ≤15 to 20 μm in maximum size, and they are often recrystallized. Thus, only few of them were measurable. Host-mineral compositions are given in Table S2. All melt inclusions have a homogeneous rhyolitic composition, regardless of the eruption and the host mineral (Figure 2). Their alkali content ($Na_2O + K_2O$) varies from 4 to 7 wt %, with most inclusions having concentrations between 6 and 7 wt%. Their melt inclusion SiO_2 content varies from 71 to 79 wt%, with most values lying between 75 and 78 wt%. Melt inclusions plot in the medium-K subalkali compositional field, as shown in the K_2O versus SiO_2 plot (Figure 3a). The composition of residual
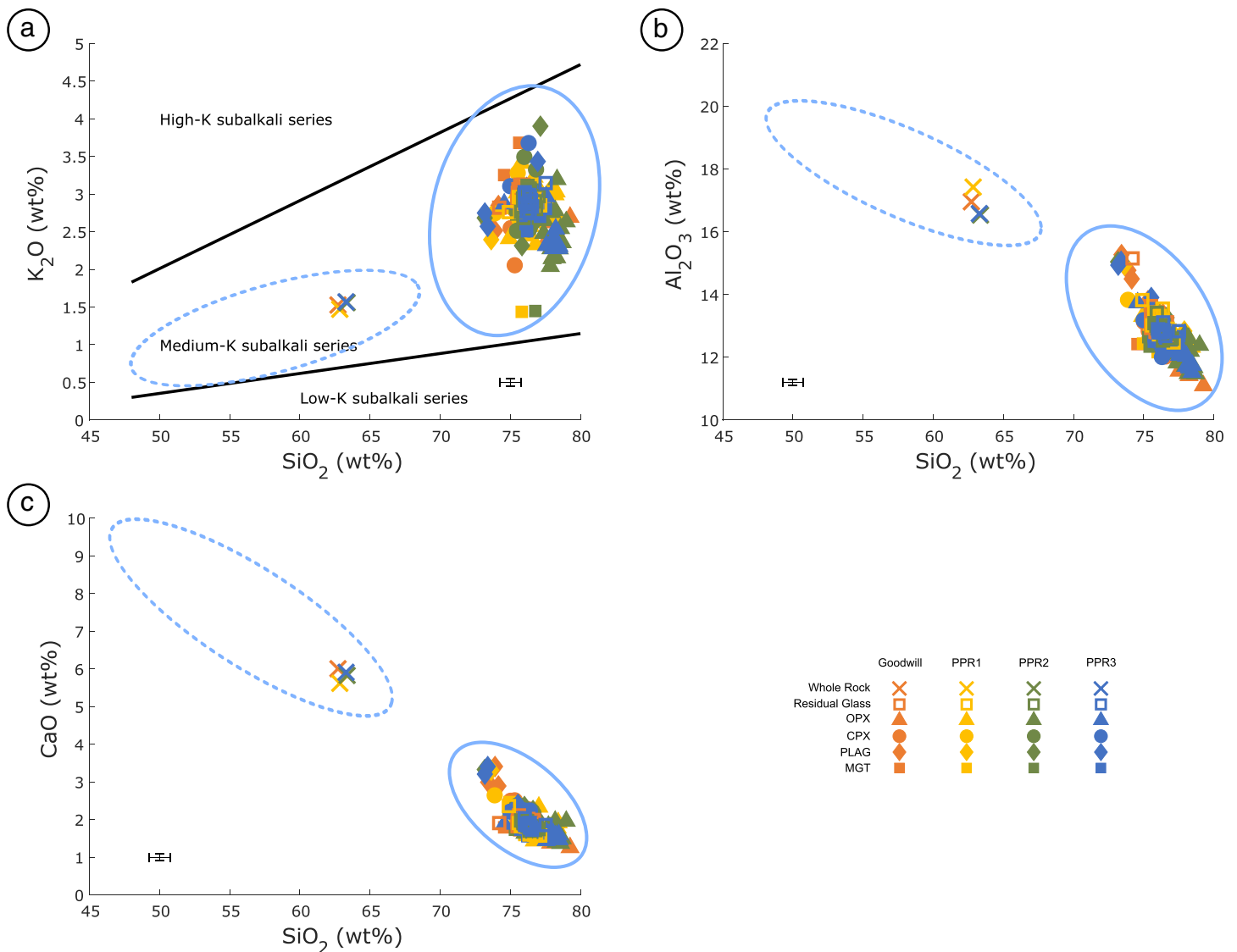
Figure 3. (a) K$_2$O versus SiO$_2$; (b) Al$_2$O$_3$ versus SiO$_2$; and (c) CaO versus SiO$_2$ for analyzed melt inclusions. The solid blue circle and the dashed blue circle mark domains of ignimbrite melt inclusion and whole rocks compositions, respectively (from Balcone-Boissard et al., 2018).

matrix glasses encompasses the range of melt inclusion compositions, as shown in Al$_2$O$_3$ and CaO and versus SiO$_2$ compositions (Figures 2 and 3). Difference in composition between whole rocks and melt inclusions can be explained by mass balance between liquid (melt inclusions) composition and crystal compositions, assuming 25% to 30% crystallization, as observed in previous ignimbritic eruption.

4.3. Melt Inclusion Host-Mineral Composition

The mineralogy of the magma emitted during the four eruptions is very similar, and similar to that of the ignimbrites (Balcone-Boissard et al., 2018): In decreasing order of abundance, PLAG, OPX, CPX, and MGT are present as phenocrysts in the magmas. Their composition is given in Table S2. Most of PLAG show strong zoning, resulting from a complex crystallization history. Half of OPX and CPX are unzoned. All MGT crystals are totally limpid. These crystals have a size between approximately 100 μm and nearly a centimeter in length. Microliths are rare, perhaps as a result of the rapid quenching of the pumice during the eruption. Scarce amphibole was also found in PPR1 and PPR3, but no melt inclusions in amphibole were characterized. Table 1 gives the enstatite (En) content range of OPX; the wollastonite (Wo) content range of CPX; the anorthite (An) content range of PLAG; and the Fe/(Fe + Ti) range of MGT.

Table 1
Host-Mineral Compositional Range

	OPX (mol% En)	CPX (mol% Wo)	PLAG (mol% An)	MGT (mol% Fe/Fe + Ti)
Goodwill	51–54	41–44	47–68	47–87
	$n = 10$	$n = 13$	$n = 8$	$n = 3$
PPR1	50–55	43–44	44–68	46–86
	$n = 32$	$n = 10$	$n = 6$	$n = 10$
PPR2	51–56	43–44	42–70	46–87
	$n = 20$	$n = 9$	$n = 9$	$n = 9$
PPR3	51–54	38–44	52–80	46–87
	$n = 11$	$n = 10$	$n = 3$	$n = 8$

Note. n is the number of melt inclusion host minerals.

4.4. Magma Temperature

Equilibrium temperatures (Table 2) for melt inclusions and their host OPX, CPX, and PLAG and for two pyroxenes (OPX-CPX) have been calculated using the thermometers of Putirka (2008): OPX-liquid (Equation 28a), CPX-liquid (Equation 33), PLAG-liquid (Equation 24a), and OPX-CPX equilibrium (Equation 37). Equilibrium temperatures for MGT-ilmenites (ILM) were calculated following Sauerzapf et al. (2008). Standard deviations of the estimates reported by Putirka (2008) are ±41°C, 42°C, 36°C, and 60°C, respectively.

Each of the crystal-melt thermometers requires an estimate of melt H_2O content and crystal and melt inclusion composition. The OPX-CPX thermometer, in contrast, requires input of OPX and CPX compositions only. The PLAG-melt thermometer also requires an estimate for the crystallization pressure. For the other thermometers, pressure and temperature can be iteratively calculated from the same compositions. For crystal-melt thermometers, the mineral composition was measured close to the analyzed melt inclusion. In case of OPX-CPX thermometer, core compositions were measured. The CPX-liquid and the OPX-CPX thermometers give similar values; the OPX-liquid thermometer gives values higher than the OPX-CPX and CPX-liquid thermometers, but with a similar deviation. The PLAG-liquid thermometer calculates values higher than the other thermometers, yet within the uncertainty of the methods, and also a larger range of temperatures. Only five MGT-ILM touching pairs were found in our samples from phenocrysts of three eruptions (Goodwill: three couples; PPR1: one couple; and PPR3: one couple). The standard error of the estimates is 50°C (Sauerzapf et al., 2008).

4.5. Volatile Contents
4.5.1. Volatile Contents in Melt Inclusions

Volatile contents detected in melt inclusions in OPX, CPX, and PLAG are shown in Figure 4, and they are listed in supporting information (Table S2).

Detected water contents in melt inclusions range between 0.77 ± 0.01 and 3.25 ± 0.01 wt% (Figures 4a, 5a, and 5b). The concentrations in OPX- and CPX-hosted melt inclusions show values that are slightly higher

Table 2
Equilibrium Temperatures Calculated Using the Thermometers Proposed by Putirka (2008) and Sauerzapf et al. (2008)

	OPX-liquid	CPX-liquid	PLAG-liquid	OPX-CPX	MGT-ILM
Goodwill	895 ± 9°C	868 ± 8°C	936 ± 23°C	865 ± 16°C	801 ± 2°C
	$n = 5$	$n = 8$	$n = 8$	$n = 5$	$n = 3$
PPR1	893 ± 9°C	869 ± 7°C	911 ± 19°C	868 ± 11°C	796°C
	$n = 9$	$n = 6$	$n = 6$	$n = 6$	$n = 1$
PPR2	893 ± 10°C	863 ± 8°C	921 ± 21°C	869 ± 12°C	
	$n = 12$	$n = 9$	$n = 8$	$n = 9$	
PPR3	886 ± 6°C	867 ± 5°C	980 ± 58°C	874 ± 33°C	784°C
	$n = 4$	$n = 10$	$n = 3$	$n = 10$	$n = 1$

Note. The reported values are mean temperatures and extreme calculated values.
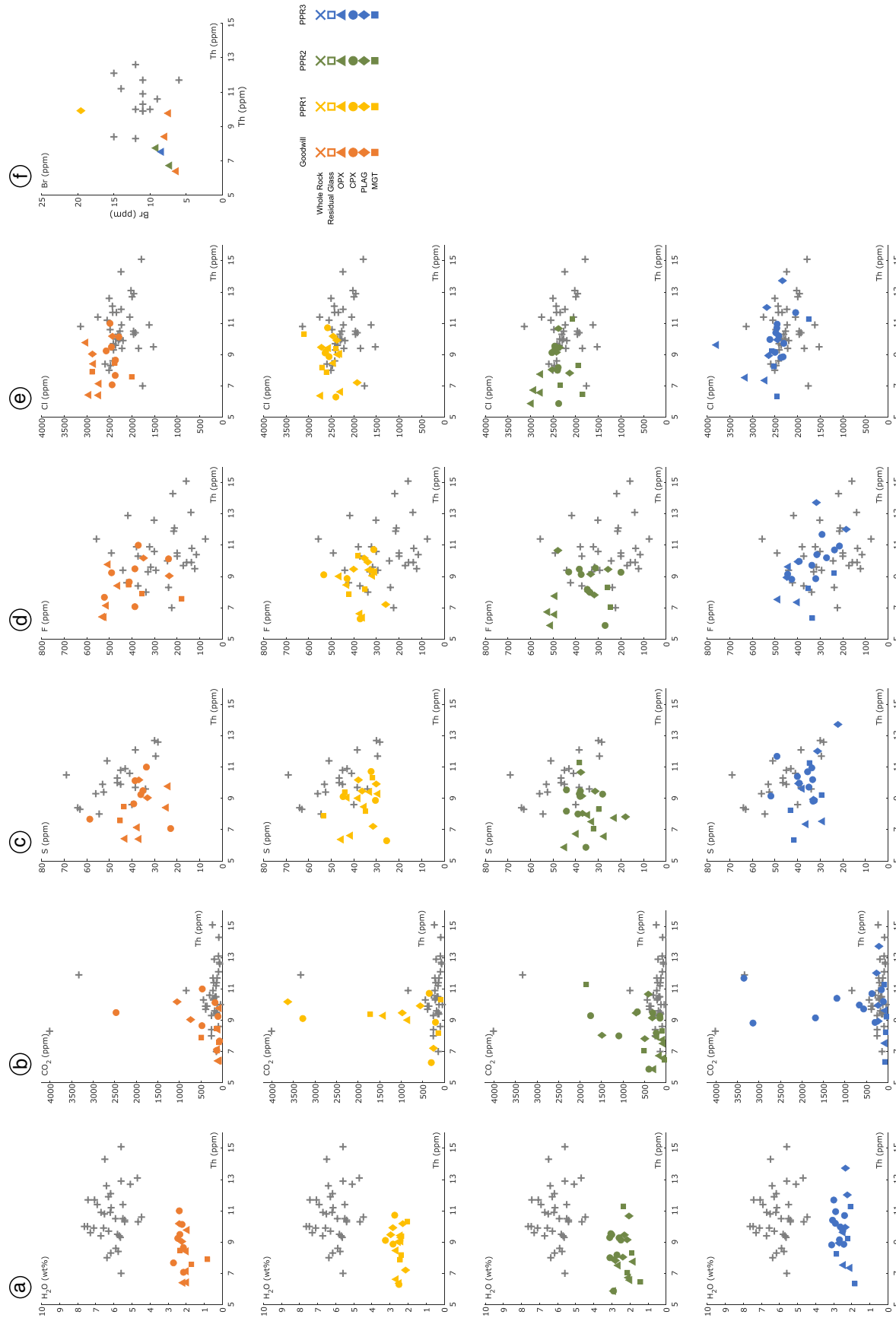
Figure 4. (a) H_2O versus Th for Goodwill, PPR1, PPR2, and PPR3; (b) CO_2 versus Th for Goodwill, PPR1, PPR2, and PPR3; (c) S versus Th for Goodwill, PPR1, PPR2, and PPR3; (d) F versus Th for Goodwill, PPR1, PPR2, and PPR3; (e) Cl versus Th for Goodwill, PPR1, PPR2, and PPR3; and (f) Br versus Th for all eruptions in one graph.
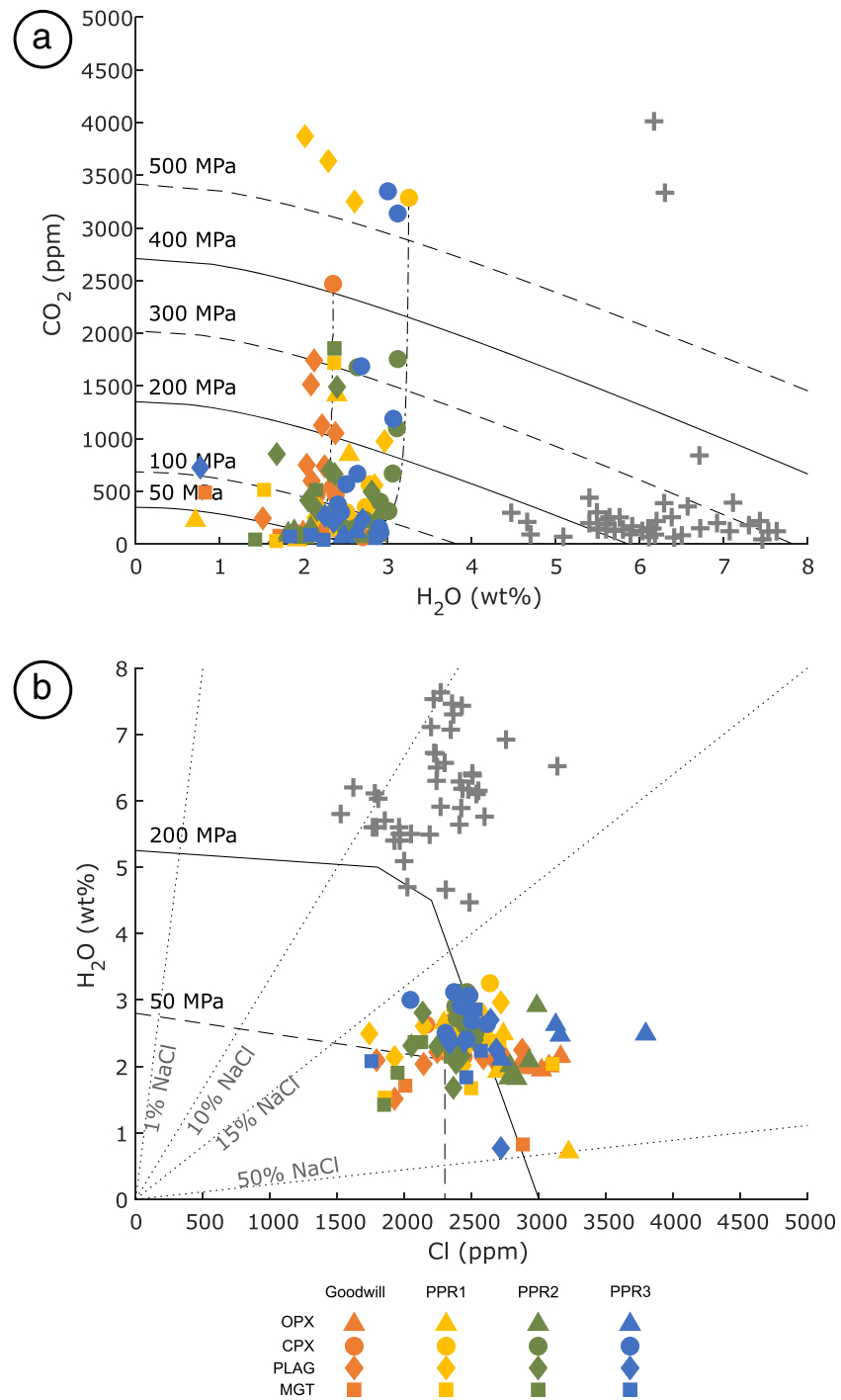
Figure 5. (a) CO_2 and H_2O contents in melt inclusions. Gray crosses mark the composition of melt inclusions in Dominica's ignimbrites (Balcone-Boissard et al., 2018). Isobars were calculated using VolatileCalc (Newman & Lowenstern, 2002) for rhyolite and a temperature of 870°C. As these isobars were calculated for a mean rhyolitic composition, they only give qualitative information. The dashed-dotted line corresponds to a 1% exsolution degassing path, calculated with VolatileCalc (Newman & Lowenstern, 2002). (b) H_2O versus Cl concentrations in melt inclusions. The gray crosses mark the composition of melt inclusions in Dominica's main ignimbrite units (Balcone-Boissard et al., 2018). Dotted lines give the weight percentage of NaCl in aqueous fluids required to produce the observed Cl/H_2O ratios.

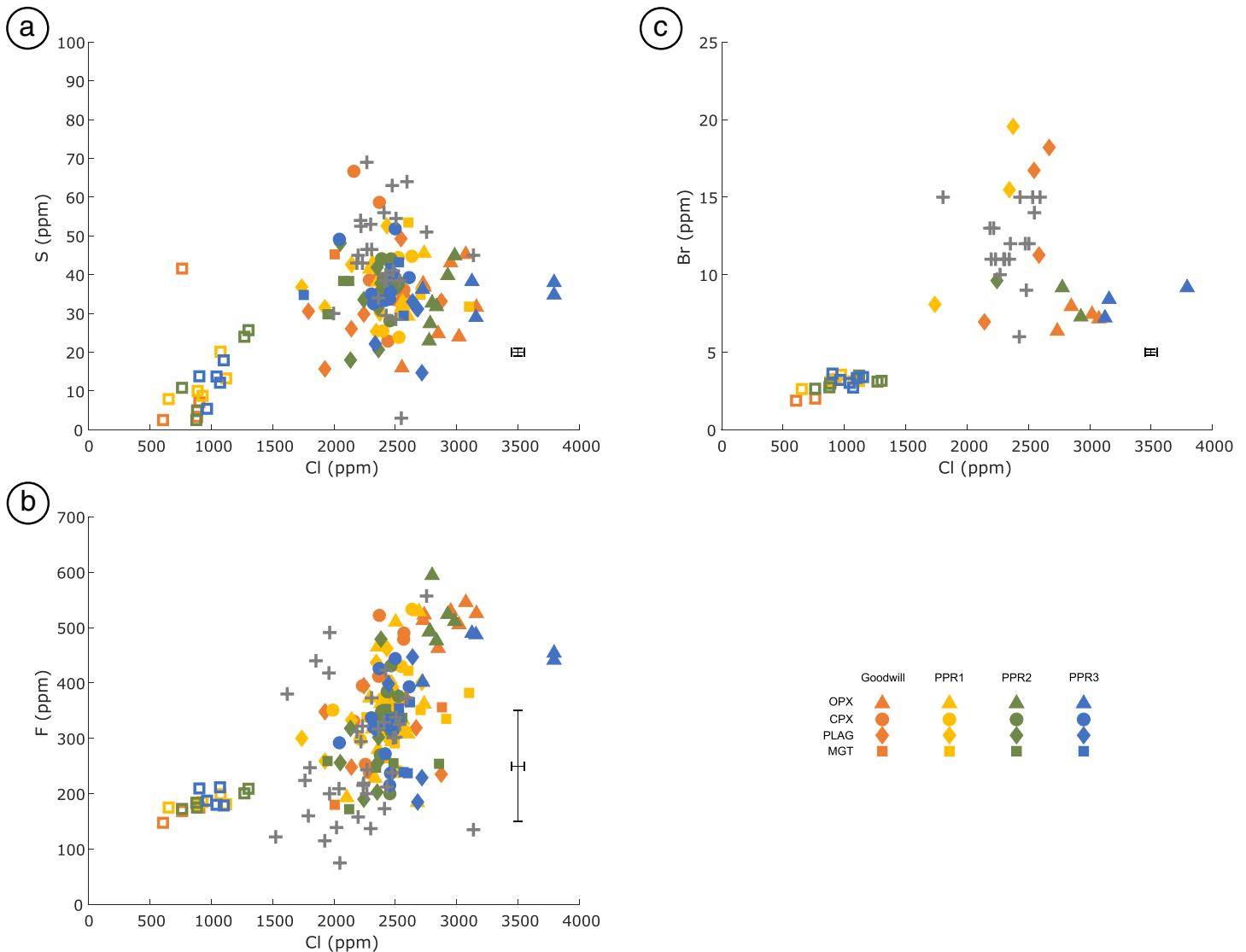**Figure 6.** (a) S versus Cl concentrations. (b) F versus Cl concentrations. (c) Br versus Cl concentrations. Gray crosses correspond to melt inclusion compositions in ignimbrites (Balcone-Boissard et al., 2018). Error bars are associated to melt inclusion values; uncertainties associated to residual glass are smaller than data points.

(1.82 $\pm$ 0.02 to 3.25 $\pm$ 0.01 wt%) than those of melt inclusions hosted by PLAG and MGT (0.77 $\pm$ 0.01 to 2.86 $\pm$ 0.05 wt%). Regardless of the host mineral, concentrations are similar for the different eruptions.

Carbon dioxide concentrations in melt inclusions are highly variable depending on the host mineral. Melt inclusions in MGT and OPX show the lowest CO_2 values, virtually all of them being below 1,000 ppm for all eruptions (Figures 4b and 5a). Only two melt inclusions trapped in MGT show concentrations as high as 1,719 $\pm$ 40 ppm (PPR1) and 1,856 $\pm$ 99 ppm (PPR2). In melt inclusions in CPX and PLAG, CO_2 concentrations are mainly between 100 and 2,000 ppm, but in PPR1 and PPR3, some melt inclusions comprise between 3,000 and 4,000 ppm CO_2 (Figures 4b and 5a). As the $^{12}C/^{18}O$ signal was stable during the analysis, the data are considered to represent true variation.

The sulfur content in the melt inclusions is lower than 60 ppm, and most of the values are between 40 and 50 $\pm$ 0.8 ppm in OPX, CPX, and PLAG from all eruptions. Our analyses of sulfur contents in melt inclusions contained in MGT are too limited to be conclusive.

Fluorine concentrations range between 172 and 594 $\pm$ 163 ppm for all eruptions. The CPX- and PLAG-hosted inclusions from all eruptions, as well as the OPX-hosted inclusions from PPR1, are mostly

between ~300 and 400 ppm. The OPX-hosted inclusions from the other eruptions, however, show F contents of mostly ~400 and 600 ppm. The MGT-hosted inclusions from PPR1 also show F contents mostly between 300 and 400 ppm, but between 200 and 300 ppm for the PPR2 and PPR3 inclusions. Analyzed melt inclusions in MGT from Goodwill are not numerous enough to be conclusive.

Chlorine concentrations in melt inclusions range between 1,226 and 3,794 $\pm$ 58 ppm for all eruptions. MGT-hosted inclusions from Goodwill, PPR1, and PPR2 have predominantly between 2,000 and 2,500 ppm of Cl; those from PPR3 show Cl contents of mostly 2,500–3,000 ppm. PLAG-hosted inclusions from PPR1 and PPR2 predominantly have 2,000–2,500 ppm of Cl, while those from Goodwill and PPR3 have mostly 2,500–3,000 ppm. In CPX, inclusions from Goodwill, PPR2, and PPR3 mostly contain 2,000 to 2,500 ppm of Cl, whereas PPR1 inclusions mostly have 2,500 to 3,000 ppm. In OPX, inclusions from Goodwill and PPR2 mainly contain 2,500–3,000 ppm of Cl; those from PPR1 more commonly have 2,000–2,500 ppm of Cl, and those from PPR3 show the widest range in Cl contents, ranging from 1,000 to 4,000 ppm.

Bromine measurements were carried out on OPX- and PLAG-hosted melt inclusions. OPX-hosted inclusions have concentrations from 6.0 $\pm$ 0.2 to 10.0 $\pm$ 0.6 ppm in all eruptions; PLAG-hosted inclusions show concentrations between 7.0 $\pm$ 0.5 and 20.0 $\pm$ 5.5 ppm of Br.

4.5.2. Volatile Contents in Residual Glasses

Water and carbon dioxide concentrations could not be measured in the matrix glasses by SIMS due to the small-size glass area.

Halogen and sulfur contents in residual glasses were calculated from the concentration obtained through pyrohydrolysis on whole rocks (Table S1) and corrected for crystal content. The calculated compositions are comparable for the different eruptions. F concentrations range between 148 $\pm$ 3 and 212 $\pm$ 7 ppm. Cl concentrations vary between 606 $\pm$ 2 and 1,304 $\pm$ 1 ppm. Br concentrations range between 1.9 $\pm$ 0.1 and 3.24 $\pm$ 0.1 ppm, and S concentrations between 3 and 42 $\pm$ 3 ppm.

4.6. Trace Element Contents in Melt Inclusions

Trace element compositions are reported in Table S3. The high field strength elements (HFSEs) show a strong correlation in melt inclusions, as shown for U and Th ([U] = 0.32*[Th]) (Figure S7). Melt inclusions hosted in all mineral types and from all eruptions show comparable compositions and compositional trends with 5 to 12 ppm of Th and 1.7 to 3.7 ppm of U. Only few melt inclusions in PLAG from PPR3 have higher concentrations, up to 20 ppm of Th and 7 ppm of U. Li concentrations vary between 5 and 15 ppm, regardless the eruption and the host mineral.

5. Discussion

5.1. Magmas Storage Conditions for Goodwill, PPR1, PPR2, and PPR3

5.1.1. Temperatures

The pre-eruptive magma storage temperatures calculated using the OPX-CPX thermometer (from 865 $\pm$ 60°C for PPR3 to 874 $\pm$ 60°C for PPR1) and the CPX-melt thermometer (from 863 $\pm$ 42°C for PPR2 to 869 $\pm$ 42°C for PPR1) are close to the pre-eruptive temperatures inferred by Gurenko et al. (2005) and Lindsay, Trumbull, et al. (2005) for silicic lavas from the PPVC (760–880°C and 800–890°C, respectively), and considering uncertainties, similar to the ~850 $\pm$ 25°C proposed by Solaro et al. (2019) for the magmas that fueled the ignimbrite eruptions from the same eruptive centers (i.e., Morne Diablotins and MTPM). The OPX-CPX and CPX-melt equilibria give the results the most consistent with previous studies carried out in this area (Balcone-Boissard et al., 2018; Gurenko et al., 2005; Lindsay, Trumbull, et al., 2005; Solaro et al., 2019). OPX-melt thermometer calculates temperatures slightly hotter than those obtained by OPX-CPX and CPX-melt thermometers (from 886°C for PPR3 to 895°C for Goodwill), but within the uncertainties of the methods. Crystallization temperatures calculated using the PLAG-melt thermometer are higher than those of OPX-melt; they range between 914 $\pm$ 36°C (PPR1) and 976 $\pm$ 36°C (PPR3). Yet these thermometric results may be taken with caution, since PLAG shows strong compositional zonings (Figure S3) that indicate a much more complicated crystallization history than for OPX. The apparently higher equilibration temperatures of some PLAG and their melt inclusions may also indicate that some PLAG crystals are antecrysts that derive from a higher temperature recharge magma that was added to

the reservoir shortly prior to eruption, but a more likely explanation is that the input H_2O contents used for the thermometric calculations are slight underestimates compared to saturation H_2O values. Underestimated melt H_2O contents strongly increase calculated PLAG-liquid temperatures, but they only slightly increase the other calculated crystal-liquid temperatures (Putirka, 2008). The PLAG-melt thermometric estimates are therefore not likely to be representative for the pre-eruptive storage conditions. The MGT-ILM thermometry indicates equilibration about 100°C lower than for the other equilibria. Regardless of our limited data set, we attribute this difference to re-equilibration during cooling, for example, during ascent. In summary, the results of the thermometry thus suggest pre-eruptive temperatures between 860°C and 890°C.

5.1.2. Fluids in the Reservoir

Degassing paths calculated with the VolatileCalc rhyolite solubility model (Newman & Lowenstern, 2002) indicate closed-system degassing with 0% exsolution (Goodwill and PPR2) or 1% exsolution (PPR1 and PPR3; Figure 5a). Furthermore, some melt inclusions contain high CO_2 concentrations (3,000 to 4,000 ppm) but comparatively low H_2O concentrations (<2.7 wt%) and therefore very low $H_2O/(H_2O + CO_2)$ ratios. Balcone-Boissard et al. (2018) also observed such high CO_2 contents in melt inclusions from MTPM ignimbrites. Caricchi et al. (2018) attributed this phenomenon to CO_2 flushing from deep levels within the magma plumbing system, driving melt dehydration and crystallization at shallower levels. Following this interpretation, high CO_2-low H_2O compositions detected in melt inclusions from Dominica could be attributed to water loss triggered by the flushing of magmas stored at shallow depths by ascending CO_2-rich fluid phase degassed from deeper magma. High CO_2 degassing is observed within the valley of Desolation as evidenced by Di Napoli et al. (2013). It would be consistent with a transcrustal magma system composed of various storage depths.

Chlorine content in melt inclusions is independent of Th concentration, which is a marker of a buffering effect on Cl concentration of silicate melt (Figure 4). Signorelli and Carroll (2002) have shown that in phonolites at pressures lower than 200 MPa, Cl concentration is buffered by a three-phase system of silicate melt, a hydrous vapor, and a brine. This buffer maintains a constant Cl concentration in the melt. Balcone-Boissard et al. (2016) have observed a similar Cl buffering phenomenon in phonolitic and trachytic residual glasses from Vesuvius. It is thus reasonable to posit that Cl is buffered in the rhyolitic melt involved in the studied eruptions and stored under pressures of ≤ ~200 MPa. Part of Cl is thus partitioned into the fluid phase.

Figures 6b and 6c show that F and Br concentrations decrease for a constant Cl concentration in melt inclusions, interpreted to record Cl buffering in the presence of Cl-rich brine (Balcone-Boissard et al., 2016). Residual glasses have the same F/Cl and Br/Cl ratios as the most F-depleted and Br-depleted melt inclusions, which suggests that the degassing behavior during ascent remains in equilibrium. Otherwise, residual glasses would have different halogen ratios than the melt inclusions, though they define low-value end-members.

S/Cl ratio is largely invariant for the analyzed melt inclusions and residual glasses, yet somewhat higher in the melt inclusions (Figure 6a). Sulfur concentrations are low, even in melt inclusions, and they show no clear trend. Sulfur seems to be almost totally exsolved from the melt before melt inclusion entrapment, or poorly concentrated in the source and the magmas. That is why S degassing budgets appear to be quite low and more variable than the ones for the halogens: They range from 3.06×10^{-2} Mt/km^3 (Goodwill) to 6.92×10^{-2} Mt/km^3 (Roseau). Because of the low values and the relatively high variability, it is reasonable to think that S behaves differently from the halogens. Several authors have shown that sulfur solubility is low in felsic magmas and easily exsolves from the silicate melt to a fluid phase (e.g., Gerlach et al., 1996; Scaillet et al., 1998; Wallace, 2005). It is likely that the sulfur has partitioned into a fluid phase, probably the same one that also buffers chlorine. However, we cannot exclude that S underwent at least partial passive degassing. Therefore, calculated emissions of S are likely to give only a minimum value.

5.1.3. Storage Pressures and Depths

The solubility of H_2O-CO_2-dominated fluids for a given temperature and melt composition largely depends on the storage pressure. Thus, if the magma is fluid saturated, the measured H_2O-CO_2 concentration provides constraints on magma pressure when the melt inclusion was trapped. MagmaSat (Ghiorso & Gualda, 2015) was used to calculate fluid-saturation pressures for each melt inclusion composition. The

Table 3
Halogen Emissions for the Eruptions Studied in This Article and Those Found in Literature

	Min vol magma (km^3)	Max vol magma (km^3)	S min (Mt/km^3)	S max (Mt/km^3)	F min (Mt/km^3)	F max (Mt/km^3)	Cl min (Mt/km^3)	Cl max (Mt/km^3)	Br min (Mt/km^3)	Br max (Mt/km^3)	Ref.
Dominica											
Layou, 50.6 ka BP	3.00	5.00	0.02	0.05	0.00	0.14	0.47	1.56	0.01	0.03	1
Roseau, 33.3 ka BP	3.00	5.00	0.00	0.07	0.00	0.26	0.68	2.85	0.03	0.04	1
Grand-Fond, 24 ka BP	3.00	5.00	0.02	0.05	0.00	0.22	0.35	1.47	0.02	0.03	1
Goodwill, 18.1 ka BP	0.30	0.50	0.00	0.03	0.01	0.27	2.12	3.96	0.01	0.02	1
PPR1, 12.6 ka BP	0.30	0.50	0.00	0.04	0.00	0.25	0.86	2.70			1
PPR2, 12.5 ka BP	0.30	0.50	0.00	0.05	0.00	0.28	0.76	2.29	0.01	0.02	1
PPR3, 9.4 ka BP	0.30	0.50	0.00	0.05	0.00	0.20	0.32	3.78	0.01	0.02	1

	Magma (km^3)		S min (Mt/km^3)	S max (Mt/km^3)	F min (Mt/km^3)	F max (Mt/km^3)	Cl min (Mt/km^3)	Cl max (Mt/km^3)	Br min (Mt/km^3)	Br max (Mt/km^3)	Ref.
Other eruptions											
Santorini 39 ka BP	39		0.01	0.92	0.58	0.61	1.30	17.31	0.00	0.04	2
Samalas 1215 AD	37–43		1.70	2.30			5.65	5.70	0.03	0.04	3
Tambora 1815 AD	30		0.88	0.97		3.99		7.00			4; 5; 6
Krakatau 1883 AD	4			0.24				0.91			5, 6
Soufrière Hills 20/05/2006	0.02		4.50	5.51			0.15	0.49			7; 8
Mt St Helens 1980 AD	0.24–0.40		1.88	3.10							4; 9; 10

Note. When values are given as gas molecule, it is considered that the element is only emitted as the given molecule, and the weight emission is then recalculated to the sole element. For instance, S is given as SO_2: $m_S = M_S * n_S = \frac{M_S}{M_{SO_2}} * m_{SO_2}$, where m is the mass and M the molar mass. It allows easier comparison of gas emissions from heterogeneous values scattered in the literature, even if it leads to a slight underestimation of the total emission for the element. References: (1) Boudon et al. (2017); (2) Cadoux et al. (2015); (3) Vidal et al. (2016); (4) Self et al. (2004); (5) Self (2006); (6) Palais and Sigurdsson (1989); (7) Wadge et al. (2010); (8) Prata et al. (2007) in Mather (2015); (9) Carey and Sigurdsson (1985); (10) Gerlach and McGee (1994).

MagmaSat calculations mostly give pressures between 50 and 150 MPa (Table S2), which corresponds to a depth range of 1.8–5.5 km, considering a mean density of 2,800 kg/m^3. The results are consistent with pressures retrieved from the H_2O-CO_2 solubility curves calculated using the VolatileCalc rhyolite solubility model (Newman & Lowenstern, 2002) for a mean temperature of 870°C (Figure 5a). Following this solubility model, the majority of the compositions give pressures between 50 and 200 MPa, that is, depths of 1.8 to 7.3 km.

Nevertheless, some melt inclusions have H_2O-CO_2 contents that indicate storage pressures much higher than 200 MPa (Figure 5a). These inclusions are trapped in PLAG with compositions (An_{53-56}) in the range of the PLAG compositions (An_{52-87}) experimentally crystallized by Solaro et al. (2019) at pressures of 300 to 400 MPa. According to the phase relations determined by Solaro et al. (2019), amphibole should however also be stable above 200 MPa (for melt H_2O contents >6 wt%). Yet amphibole is particularly scarce (<1 vol%) in magmas from the investigated plinian eruptions. Therefore, it is reasonable to consider that part of the crystal assemblage are antecrysts that grew at pressures higher than 200 MPa before ascent and storage in a shallower reservoir(s), where most of the crystals grew and where they trapped most of their melt inclusions. The H_2O content of melt inclusions trapped at deeper levels may have re-equilibrated at shallower

level, while CO_2 diffusion through PLAG or pyroxenes is exceedingly sluggish, thus preserving evidence for deeper-level crystallization.

The Cl-H_2O solubility isobars in a rhyolite melt (Webster, 1997) also give constraints on storage pressure, yet with lower precision than in the H_2O-CO_2 system (Figure 5b). Melt inclusion compositions for the four eruptions, however, equally indicate equilibration pressures between 50 and 200 MPa, and they are thus consistent with our estimates based on H_2O-CO_2 compositions.

Another way to estimate storage pressure is to compare measured volatile concentrations to solubility laws. No solubility law exist for Cl in rhyolitic liquid, but Signorelli and Carroll (2002) experimentally determined one for trachytes (which have comparable SiO_2 contents but higher alkali contents than the studied rhyolitic melts). Using this law also suggests that the highest Cl concentrations correspond to pressures of 200 MPa, that is, depths of 7.3 km.

All lines of evidence considered thus indicate that the magmas erupted in the investigated plinian eruptions were stored at maximum pressures of ~200 MPa, that is, at a depth of ≤7.3 km if we assume a mean crustal density of 2,800 kg/m^3.

5.2. Comparison With Ignimbrites in the Central Part of Dominica—Implications for the Plumbing System Architecture in Dominica

Halogen element ratios in melts depend on their magma source. Balcone-Boissard et al. (2010) have shown that the ratio is conservative during differentiation and degassing. The similar halogen signature (Figure 6), the similar major-element composition (Figures 2 and 3), and trace element ratios (Figure S7) in melt inclusions of the plinian eruptions and the ignimbrites indicate a common magma and fluid source at depth.

Balcone-Boissard et al. (2018) and Solaro et al. (2019) determined that the magma(s) feeding the ignimbrite eruptions were stored at a depth of approximately 16 km beneath Dominica. Using crustal density models of Kopp et al. (2011) and Melekhova et al. (2019) to the North of Dominica, Solaro et al. (2019) deduced that these depths correspond to the boundary between the lower and middle crusts. According to the same crustal models, our results suggest storage of the magmas that fueled the plinian eruptions at the limit between the middle and upper crusts, or within the upper crust. This suggests that the Goodwill and PPR1 to PPR3 eruptions were fed by magmas that were stored at much shallower depths than those that fueled the ignimbrite eruptions. The inferred storage conditions are close to those proposed by Gurenko et al. (2005) and Lindsay, Trumbull, et al. (2005) for the PPVC magmas, for which they estimated ~760–880°C, 200 MPa and 800–890°C, 200–300 MPa, respectively.

Such a high range of storage depths, correlated with a common magmatic source, is consistent with the transcrustal magmatic system model (Sparks & Cashman, 2017), in which crystal-rich magma mush (e.g., Cooper, 2017) extends throughout all or most of the crustal column.

5.3. Comparison With Other Islands of the Lesser Antilles Arc

The importance of shallow magma storage determined for the plinian eruptions on Dominica has also been proposed for the volcanic systems under several other islands of the Lesser Antilles arc. Beneath Montagne Pelée (Martinique), magma feeding the last eruptions has been stored at 200 ± 50 MPa and 875–900°C, according to experimental petrology investigations (Annen et al., 2008; Martel et al., 1998; Pichavant et al., 2002). Pichavant et al. (2002) also experimentally determined that more mafic magmas were stored at 400 to 500 MPa beneath Montagne Pelée. For the last dome-forming eruption of la Soufrière de Guadeloupe, the erupted magma was also stored at low pressure of 135 to 200 MPa according to experimental petrology (Pichavant et al., 2018). Devine et al. (2003) further proposed that Monserrat is underlain by several magma reservoirs differing in composition and depth. Edmonds et al. (2016) argued that beneath Montserrat, a mushy plumbing system extends from 4 to 16 km with different isolated magma bodies, and a main active reservoir located at a depth of 8–12 km.

A number of studies thus suggest that a magma ponding zone is commonly developed at a depth of approximately 5 to 8 km beneath the islands of the Lesser Antilles arc, corresponding to the limit between upper and middle crusts, according to the crust model proposed by Melekhova et al. (2019). The wide range of storage depths beneath Dominica (Balcone-Boissard et al., 2018; Solaro et al., 2019; this study), Martinique (Annen

et al., 2008; Martel et al., 1998; Pichavant et al., 2002), Guadeloupe (Pichavant et al., 2018), and Montserrat (Devine et al., 2003; Edmonds et al., 2016) is in good agreement with a transcrustal magma system (Cashman et al., 2017) and allows to suspect such plumbing systems also beneath other, less-studied islands of the Lesser Antilles arc.

5.4. Volatile Behavior and Degassing Budgets
5.4.1. Dominica

Degassing budgets were calculated from the difference in concentration between melt inclusions (pre-eruptive concentrations) and residual glasses (post-eruptive concentrations). The released mass of a volatile element X during the eruption (in kg) corresponds to the mass of X in the pre-eruptive magma ($m_X{}^{magma}$) multiplied by the degassed fraction (f_d) of X.

$$f_d = \frac{[X]^{MI} - [X]^{RG}}{[X]^{MI}} = \frac{[X]_{MI} - \left(\frac{[X]^{WR}}{f_{RG}} - [X]^{cryst} (1 - f_{RG}) \right)}{[X]^{MI}}$$

where $[X]^i$ is the molar concentration of X in the phase i, f_{RG} is the fraction of residual glass, and MI, WR, and $cryst$ are melt inclusion, whole rock, and crystal, respectively.

$$m_X^{magma} = C_X^{MI} * m_{magma} = \left(\frac{n_X * M_X}{n_{WR} * M_{WR}} \right) * m_{magma} = \left(\frac{[X]_{MI} * M_X}{10^6 * M_{WR}} \right) * m_{magma}$$

where C_X^{MI} is the massic concentration of X in the melt inclusion (the pre-eruptive magma), m_{magma} is the mass of magma, n_i is the quantity of i, and M_i is the molar mass of i.

Finally,

$$m_X = m_{magma} * \left(\frac{M_X}{10^6 * M_{WR}} \right) * \left([X]^{MI} - \frac{[X]^{WR}}{f_{RG}} + [X]^{cryst} (1 - f_{RG}) \right)$$

The precision is affected by several factors. The maximum estimations are calculated from the highest concentrations and the minimum estimations are calculated from the lowest ones, originated the range observed in Table 3. However, the major point of precision loss derives from the uncertainty on the erupted magma volume (because of erosion on land and deposits in the ocean). Boudon et al. (2017) estimated a maximum volume of 0.5 km^3 for each of the four plinian eruptions. Degassing budgets have also been calculated for the three last ignimbrite eruptions on Dominica (Layou, Roseau, and Grand-Fond), which are estimated at 3 to 5 km^3 (Boudon et al., 2017). The results are shown in Table 3. To allow comparison between eruptions, all degassing budgets were normalized to 1 km^3 of erupted magma.

The calculated mass of Cl degassing during the plinian eruptions varies between 1.47 Mt/km^3 (Grand-Fond) and 3.96 Mt/km^3 (Goodwill). However, as it appears to be buffered by a fluid phase whose Cl concentration cannot be estimated, the calculation gives a minimum value. The mass of F outgassing during eruption varies between 1.41×10^{-1} Mt/km^3 (Layou) and 2.72×10^{-1} Mt/km^3 (Goodwill). Br degassing output ranges between 1.80×10^{-2} Mt/km^3 (Goodwill) and 3.85×10^{-2} Mt/km^3 (Roseau). Volume-normalized eruptive outputs are thus comparable for the different eruptions for each halogen species. For every eruption, the Cl degassing budget is 1 order of magnitude higher than the F degassing budget and 2 orders of magnitude higher than the Br degassing budget. As S concentrations in the magma are low, degassing budgets seem low and variable: They range from 3.06×10^{-2} Mt/km^3 (Goodwill) to 6.92×10^{-2} Mt/km^3 (Roseau).

5.4.2. Comparison With Other Eruptions

Degassing budgets inferred for Dominica are here compared to those of several famous eruptions, differing in their erupted volume of magma. Unfortunately, the literature does not provide complete halogen and S data sets for these eruptions, but the main observation is that sulfur eruptive budgets of many volcanic centers are much more significant than those calculated in this study for the Dominican eruptions (ranging between 0 and 0.07 Mt/km^3, Table 3). For instance, the Minoan eruption of Santorini volcano (39 ka BP) released 0.01 to 0.92 Mt/km^3 of S (Cadoux et al., 2015), Samalas released 1.7 to 2.3 Mt/km^3 (Vidal

et al., 2016), and Soufrière Hills, Montserrat, even produced 4.5 to 5.5 Mt/km^3 of S (calculated from Prata et al., 2007; Wadge et al., 2010). Halogen data are unfortunately too scarce for differentiated magmas to highlight any clear trends, but chlorine degassing budgets are important wherever it has been measured (0.5 to 17 Mt/km^3). Estimating F and Br through halogen ratios measured for Dominica or through literature data (e.g., Cl/Br = 273, Bureau et al., 2000) gives significant degassing values, and both halogens are thus likely to be important volcanic discharge products.

6. Conclusions

Our study provides a better understanding of the crustal-scale magma plumbing system beneath the MTPM volcanic center of Dominica. The Plinian eruptions (8–18 ka) were all fed by magmas from a reservoir stored at 50–200 MPa and 860–880°C, unlike the ignimbrites that erupted between 60 and 24 ka BP, which were stored at 300–400 MPa and about 850°C. However, the similar mineralogical and chemical composition of the magmas discharged in the ignimbrites and post-ignimbrite plinian eruptions, and especially their comparable volatile element ratios, indicate a common source at depth. This common origin of the magmas from all eruptions supports a transcrustal magmatic system model.

This study also establishes volatile degassing budgets for the recent explosive eruptions of Dominica during the last 60 ka and highlights the importance of halogen element degassing. For each halogen species, the eruptive budget normalized to magma volume is of the same order of magnitude for all investigated eruptions. F and Cl eruptive emissions are 1 and 2 orders of magnitude higher than those of Br. But Cl degassing budget is a minimum value considering the partitioning into a fluid phase highlighted by melt inclusions investigation. This study highlights the necessity to take halogen species into account, in both melt inclusions and matrix glasses, when estimating degassing budgets to estimate the environmental consequences of eruptions.

Data Availability Statement

Supplementary materials are archived in the "HAL – Sorbonne Université" data repository and are available online (at https://hal.sorbonne-universite.fr/hal-02902536).

References

Aiuppa, A. (2009). Degassing of halogens from basaltic volcanism: Insights from volcanic gas observations. *Chemical Geology*, *263*(1–4), 99–109. https://doi.org/10.1016/j.chemgeo.2008.08.022

Annen, C., Pichavant, M., Bachmann, O., & Burgisser, A. (2008). Conditions for the growth of a long-lived shallow crustal magma chamber below Mount Pelee volcano (Martinique, Lesser Antilles Arc). *Journal of Geophysical Research*, *113*, B0720. https://doi.org/10.1029/2007JB005049

Bachmann, O., & Bergantz, G. (2008). The magma reservoirs that feed supereruptions. *Elements*, *4*(1), 17–21. https://doi.org/10.2113/GSELEMENTS.4.1.17

Baker, D. R. (2008). The fidelity of melt inclusions as records of melt composition. *Contributions to Mineralogy and Petrology*, *156*(3), 377–395. https://doi.org/10.1007/s00410-008-0291-3

Balcone-Boissard, H., Boudon, G., Blundy, J. D., Martel, C., Brooker, R. A., Deloule, E., et al. (2018). Deep pre-eruptive storage of silicic magmas feeding Plinian and dome-forming eruptions of central and northern Dominica (Lesser Antilles) inferred from volatile contents of melt inclusions. *Contributions to Mineralogy and Petrology*, *173*(12), 1–24. https://doi.org/10.1007/s00410-018-1528-4

Balcone-Boissard, H., Boudon, G., Cioni, R., Webster, J. D., Zdanowicz, G., Orsi, G., & Civetta, L. (2016). Chlorine as a geobarometer for alkaline magmas: Evidence from a systematic study of the eruptions of Mount Somma-Vesuvius. *Scientific Reports*, *6*(1), 1–11. https://doi.org/10.1038/srep21726

Balcone-Boissard, H., Villemant, B., & Boudon, G. (2010). Behavior of halogens during the degassing of felsic magmas. *Geochemistry, Geophysics, Geosystems*, *11*, Q09005. https://doi.org/10.1029/2010GC003028

Balcone-Boissard, H., Villemant, B., Boudon, G., & Michel, A. (2008). Non-volatile vs volatile behaviours of halogens during the AD 79 plinian eruption of Mt. Vesuvius, Italy. *Earth and Planetary Science Letters*, *269*(1), 66–79. https://doi.org/10.1016/j.epsl.2008.02.003

Balcone-Boissard, H., Villemant, B., Boudon, G., & Michel, A. (2009). *Halogen behaviours during andesitic magma degassing: From magma chamber to volcanic plume* (Vol. 11, p. 11985). Vienna, Austria: Geochemistry, Geophysics, Geosystems, AGU Pubs. Presented at the EGU general assembly conference abstracts. Retrieved from http://adsabs.harvard.edu/abs/2009EGUGA..1111985B

Boudon, G., Balcone-Boissard, H., Solaro, C., & Martel, C. (2017). Revised chronostratigraphy of recurrent ignimbritic eruptions in Dominica (Lesser Antilles arc): Implications on the behavior of the magma plumbing system. *Journal of Volcanology and Geothermal Research*, *343*, 135–154. https://doi.org/10.1016/j.jvolgeores.2017.06.022

Bouvier, A.-S., Métrich, N., & Deloule, E. (2010). Light elements, volatiles, and stable isotopes in basaltic melt inclusions from Grenada, Lesser Antilles: Inferences for magma genesis. *Geochemistry, Geophysics, Geosystems*, *11*, Q09004. https://doi.org/10.1029/2010GC003051

Bureau, H., Keppler, H., & Métrich, N. (2000). Volcanic degassing of bromine and iodine: Experimental fluid/melt partitioning data and applications to stratospheric chemistry. *Earth and Planetary Science Letters*, *183*(1), 51–60. https://doi.org/10.1016/S0012-821X(00)00258-2

Cadoux, A., Iacono-Marziano, G., Paonita, A., Deloule, E., Aiuppa, A., Nelson Eby, G., et al. (2017). A new set of standards for *in–situ* measurement of bromine abundances in natural silicate glasses: Application to SR-XRF, LA-ICP-MS and SIMS techniques. *Chemical Geology*, *452*, 60–70. https://doi.org/10.1016/j.chemgeo.2017.01.012

Cadoux, A., Scaillet, B., Bekki, S., Oppenheimer, C., & Druitt, T. (2015). Stratospheric ozone destruction by the Bronze-Age Minoan eruption (Santorini volcano, Greece). *Scientific Reports*, *5*(1), 1–12. https://doi.org/10.1038/srep12243

Cannatelli, C., Doherty, A. L., Esposito, R., Lima, A., & De Vivo, B. (2016). Understanding a volcano through a droplet: A melt inclusion approach. *Journal of Geochemical Exploration*, *171*, 4–19. https://doi.org/10.1016/j.gexplo.2015.10.003

Carey, S., & Sigurdsson, H. (1985). The May 18, 1980 eruption of Mount St. Helens: 2. Modeling of dynamics of the Plinian Phase. *Journal of Geophysical Research*, *90*(B4), 2948. https://doi.org/10.1029/JB090iB04p02948

Caricchi, L., Sheldrake, T. E., & Blundy, J. (2018). Modulation of magmatic processes by CO_2 flushing. *Earth and Planetary Science Letters*, *491*, 160–171. https://doi.org/10.1016/j.epsl.2018.03.042

Carignan, J., Hild, P., Mevelle, G., Morel, J., & Yeghicheyan, D. (2001). Routine analyses of trace elements in geological samples using flow injection and low pressure on-line liquid chromatography coupled to ICP-MS: A study of geochemical reference materials BR, DR-N, UB-N, AN-G and GH. *Geostandards Newsletter*, *25*(2–3), 187–198. https://doi.org/10.1111/j.1751-908X.2001.tb00595.x

Carroll, M. R. (2005). Chlorine solubility in evolved alkaline magmas. *Annals of Geophysics*, *48*(4/5), 619–631.

Cashman, K. V., Sparks, R. S. J., & Blundy, J. D. (2017). Vertically extensive and unstable magmatic systems: A unified view of igneous processes. *Science*, *355*(6331), eaag3055. https://doi.org/10.1126/science.aag3055

Clemente, B. (2004). The solubility of sulphur in hydrous rhyolitic melts. *Journal of Petrology*, *45*(11), 2171–2196. https://doi.org/10.1093/petrology/egh052

Cooper, K. M. (2017). What does a magma reservoir look like? The "crystal's-eye" view. *Elements*, *13*(1), 23–28. https://doi.org/10.2113/gselements.13.1.23

Danyushevsky, L. V., McNeill, A. W., & Sobolev, A. V. (2002). Experimental and petrological studies of melt inclusions in phenocrysts from mantle-derived magmas: An overview of techniques, advantages and complications. *Chemical Geology*, *183*(1), 5–24. https://doi.org/10.1016/S0009-2541(01)00369-2

Devine, J. D., Rutherford, M. J., Norton, G. E., & Young, S. R. (2003). Magma storage region processes inferred from geochemistry of Fe–Ti oxides in andesitic magma, Soufriere Hills Volcano, Montserrat, WI. *Journal of Petrology*, *44*(8), 1375–1400. https://doi.org/10.1093/petrology/44.8.1375

Di Matteo, V., Carroll, M. R., Behrens, H., Vetere, F., & Brooker, R. A. (2004). Water solubility in trachytic melts. *Chemical Geology*, *213*(1), 187–196. https://doi.org/10.1016/j.chemgeo.2004.08.042

Edmonds, M., Kohn, S. C., Hauri, E. H., Humphreys, M. C. S., & Cassidy, M. (2016). Extensive, water-rich magma reservoir beneath southern Montserrat. *Lithos*, *252–253*, 216–233. https://doi.org/10.1016/j.lithos.2016.02.026

Fearnley, C. J., Bird, D. K., Haynes, K., McGuire, W. J., & Jolly, G. (Eds) (2018). *Observing the volcano world: Volcano crisis communication*. Cham: Springer International Publishing. https://doi.org/10.1007/978-3-319-44097-2

Frey, H. M., Manon, M. R. F., Brehm, S. K., & Babiak, R. N. (2018). Episodic crystallization in young explosive eruptions in Dominica, Lesser Antilles, revealed by U-Th dating of zircons. *Geology*, *46*(10), 887–890. https://doi.org/10.1130/G45217.1

Gagnon, J. E., Fryer, B. J., Samson, I. M., & Williams-Jones, A. E. (2008). Quantitative analysis of silicate certified reference materials by LA-ICPMS with and without an internal standard. *Journal of Analytical Atomic Spectrometry*, *23*(11), 1529–1537. https://doi.org/10.1039/B801807N

Gerlach, T. M., & McGee, K. A. (1994). Total sulfur dioxide emissions and pre-eruption vapor-saturated magma at Mount St. Helens, 1980–88. *Geophysical Research Letters*, *21*(25), 2833–2836. https://doi.org/10.1029/94GL02761

Gerlach, T. M., Westrich, H. R., & Symonds, R. B. (1996). Preeruption vapor in magma of the climactic Mount Pinatubo eruption: Source of the giant stratospheric sulfur dioxide cloud. *Fire and mud: eruptions and lahars of Mount Pinatubo, Philippines*, 415, 33.

Ghiorso, M. S., & Gualda, G. A. R. (2015). An H_2O–CO_2 mixed fluid saturation model compatible with rhyolite-MELTS. *Contributions to Mineralogy and Petrology*, *169*(6), 53. https://doi.org/10.1007/s00410-015-1141-8

Gurenko, A. A., Trumbull, R. B., Thomas, R., & Lindsay, J. M. (2005). A melt inclusion record of volatiles, trace elements and Li–B isotope variations in a single magma system from the Plat Pays Volcanic Complex, Dominica, Lesser Antilles. *Journal of Petrology*, *46*(12), 2495–2526. https://doi.org/10.1093/petrology/egi063

Halama, R., Boudon, G., Villemant, B., Joron, J.-L., Le Friant, A., & Komorowski, J.-C. (2006). Pre-eruptive crystallization conditions of mafic and silicic magmas at the Plat Pays volcanic complex, Dominica (Lesser Antilles). *Journal of Volcanology and Geothermal Research*, *153*(3), 200–220. https://doi.org/10.1016/j.jvolgeores.2005.12.001

Harms, E., & Schmincke, H.-U. (2000). Volatile composition of the phonolitic Laacher See magma (12,900 yr BP): Implications for syn-eruptive degassing of S, F, Cl and H_2O. *Contributions to Mineralogy and Petrology*, *138*(1), 84–98. https://doi.org/10.1007/PL00007665

Howe, T. M., Lindsay, J. M., & Shane, P. (2015). Evolution of young andesitic–dacitic magmatic systems beneath Dominica, Lesser Antilles. *Journal of Volcanology and Geothermal Research*, *297*, 69–88. https://doi.org/10.1016/j.jvolgeores.2015.02.009

Howe, T. M., Lindsay, J. M., Shane, P., Schmitt, A. K., & Stockli, D. F. (2014). Re-evaluation of the Roseau Tuff eruptive sequence and other ignimbrites in Dominica, Lesser Antilles. *Journal of Quaternary Science*, *29*(6), 531–546. https://doi.org/10.1002/jqs.2723

Jochum, K. P., Stoll, B., Herwig, K., Willbold, M., Hofmann, A. W., Amini, M., et al. (2006). MPI-DING reference glasses for in situ microanalysis: New reference values for element concentrations and isotope ratios: MPI-DING reference glasses. *Geochemistry, Geophysics, Geosystems*, *7*, Q02008. https://doi.org/10.1029/2005GC001060

Kent, A. J. R. (2008). Melt inclusions in basaltic and related volcanic rocks. *Reviews in Mineralogy and Geochemistry*, *69*(1), 273–331. https://doi.org/10.2138/rmg.2008.69.8

Kopp, H., Weinzierl, W., Becel, A., Charvis, P., Evain, M., Flueh, E. R., et al. (2011). Deep structure of the central Lesser Antilles Island Arc: Relevance for the formation of continental crust. *Earth and Planetary Science Letters*, *304*(1), 121–134. https://doi.org/10.1016/j.epsl.2011.01.024

Le Friant, A., Boudon, G., Komorowski, J.-C., & Deplus, C. (2002). L'île de la Dominique, à l'origine des avalanches de débris les plus volumineuses de l'arc des Petites Antilles. *Comptes Rendus Geoscience*, *334*(4), 235–243. https://doi.org/10.1016/S1631-0713(02)01742-X

Lindsay, J. M., Smith, A. L., Roobol, M. J., & Stasiuk, M. V. (2005). Dominica. *Volcanic hazard atlas of the Lesser Antilles* (pp. 1–48).

Lindsay, J. M., Trumbull, R. B., & Siebel, W. (2005). Geochemistry and petrogenesis of late Pleistocene to Recent volcanism in Southern Dominica, Lesser Antilles. *Journal of Volcanology and Geothermal Research*, *148*(3), 253–294. https://doi.org/10.1016/j.jvolgeores.2005.04.018

Lindsay, J. M., Stasiuk, M. V., & Shepherd, J. B. (2003). Geological history and potential hazards of the late-Pleistocene to Recent Plat Pays volcanic complex, Dominica, Lesser Antilles. *Bulletin of Volcanology*, *65*(2–3), 201–220. https://doi.org/10.1007/s00445-002-0253-y

Macdonald, R., Hawkesworth, C. J., & Heath, E. (2000). The Lesser Antilles volcanic chain: A study in arc magmatism. *Earth-Science Reviews*, *49*(1–4), 1–76. https://doi.org/10.1016/S0012-8252(99)00069-0

Martel, C., Pichavant, M., Bourdier, J.-L., Traineau, H., Holtz, F., & Scaillet, B. (1998). Magma storage conditions and control of eruption regime in silicic volcanoes: Experimental evidence from Mt. Pelée. *Earth and Planetary Science Letters*, *156*(1), 89–99. https://doi.org/10.1016/S0012-821X(98)00003-X

Mather, T. A. (2015). Volcanoes and the environment: Lessons for understanding Earth's past and future from studies of present-day volcanic emissions. *Journal of Volcanology and Geothermal Research*, *304*, 160–179. https://doi.org/10.1016/j.jvolgeores.2015.08.016

Melekhova, E., Schlaphorst, D., Blundy, J., Kendall, J.-M., Connolly, C., McCarthy, A., & Arculus, R. (2019). Lateral variation in crustal structure along the Lesser Antilles arc from petrology of crustal xenoliths and seismic receiver functions. *Earth and Planetary Science Letters*, *516*, 12–24. https://doi.org/10.1016/j.epsl.2019.03.030

Métrich, N., & Deloule, E. (2014). Water content, δD and δ^{11}B tracking in the Vanuatu arc magmas (Aoba Island): Insights from olivine-hosted melt inclusions. *Lithos*, *206–207*, 400–408. https://doi.org/10.1016/j.lithos.2014.08.011

Métrich, N., & Wallace, P. J. (2008). Volatile abundances in basaltic magmas and their degassing paths tracked by melt inclusions. *Reviews in Mineralogy and Geochemistry*, *69*(1), 363–402. https://doi.org/10.2138/rmg.2008.69.10

Michel, A., & Villemant, B. (2003). Determination of halogens (F, Cl, Br, I), sulfur and water in seventeen geological reference materials. *Geostandards Newsletter*, *27*(2), 163–171. https://doi.org/10.1111/j.1751-908X.2003.tb00643.x

Miller, C. F., & Wark, D. A. (2008). Supervolcanoes and their explosive supereruptions. *Elements*, *4*(1), 11–15. https://doi.org/10.2113/GSELEMENTS.4.1.11

Napoli, R. D., Aiuppa, A., & Allard, P. (2013). First Multi-GAS based characterisation of the Boiling Lake volcanic gas (Dominica, Lesser Antilles), 13.

Newman, S., & Lowenstern, J. B. (2002). VolatileCalc: A silicate melt–H_2O–CO_2 solution model written in Visual Basic for Excel. *Computers & Geosciences*, *28*(5), 597–604. https://doi.org/10.1016/S0098-3004(01)00081-4

Palais, J. M., & Sigurdsson, H. (1989). Petrologic evidence of volatile emissions from major historic and pre-historic volcanic eruptions. In *Understanding climate change* (Vol. 52, pp. 31–53). American Geophysical Union (AGU). https://doi.org/10.1029/GM052p0031

Papale, P. (1997). Modeling of the solubility of a one-component H_2O or CO_2 fluid in silicate liquids. *Contributions to Mineralogy and Petrology*, *126*(3), 237–251. https://doi.org/10.1007/s004100050247

Pichavant, M., Martel, C., Bourdier, J. L., & Scaillet, B. (2002). Physical conditions, structure, and dynamics of a zoned magma chamber: Mount Pelée (Martinique, Lesser Antilles Arc). *Journal of Geophysical Research*, *107*(B5). https://doi.org/10.1029/2001JB000315

Pichavant, M., Poussineau, S., Lesne, P., Solaro, C., & Bourdier, J.-L. (2018). Experimental parametrization of magma mixing: Application to the AD 1530 eruption of La Soufrière, Guadeloupe (Lesser Antilles). *Journal of Petrology*, *59*(2), 257–282. https://doi.org/10.1093/petrology/egy030

Portnyagin, M., Almeev, R., Matveev, S., & Holtz, F. (2008). Experimental evidence for rapid water exchange between melt inclusions in olivine and host magma. *Earth and Planetary Science Letters*, *272*(3), 541–552. https://doi.org/10.1016/j.epsl.2008.05.020

Prata, A. J., Carn, S. A., Stohl, A., & Kerkmann, J. (2007). Long range transport and fate of a stratospheric volcanic cloud from Soufrière Hills volcano, Montserrat. *Atmospheric Chemistry and Physics, European Geosciences Union*, *7*(19), 5093–5103.

Putirka, K. D. (2008). Thermometers and barometers for volcanic systems. *Reviews in Mineralogy and Geochemistry*, *69*(1), 61–120. https://doi.org/10.2138/rmg.2008.69.3

Roberts, T. J., Braban, C. F., Martin, R. S., Oppenheimer, C., Adams, J. W., Cox, R. A., et al. (2009). Modelling reactive halogen formation and ozone depletion in volcanic plumes. *Chemical Geology*, *263*(1), 151–163. https://doi.org/10.1016/j.chemgeo.2008.11.012

Robock, A. (2015). Climatic impacts of volcanic eruptions. In *The encyclopedia of volcanoes* (pp. 935–942). Academic Press. https://doi.org/10.1016/B978-0-12-385938-9.00053-5

Roobol, M. J., Wright, J. V., & Smith, A. L. (1983). Calderas or gravity-slide structures in the Lesser Antilles island arc? *Journal of Volcanology and Geothermal Research*, *19*(1), 121–134. https://doi.org/10.1016/0377-0273(83)90128-2

Sauerzapf, U., Lattard, D., Burchard, M., & Engelmann, R. (2008). The titanomagnetite–ilmenite equilibrium: New experimental data and thermo-oxybarometric application to the crystallization of basic to intermediate rocks. *Journal of Petrology*, *49*(6), 1161–1185. https://doi.org/10.1093/petrology/egn021

Scaillet, B., Clemente, B., Evans, B. W., & Pichavant, M. (1998). Redox control of sulfur degassing in silicic magmas. *Journal of Geophysical Research*, *103*(B10), 23,937–23,949. https://doi.org/10.1029/98JB02301

Schmidt, A., & Robock, A. (2015). Volcanism, the atmosphere and climate through time. In A. Schmidt, K. E. Fristad, & L. T. Elkins-Tanton (Eds.), *Volcanism and global environmental change* (pp. 195–207). Cambridge: Cambridge University Press. https://doi.org/10.1017/CBO9781107415683.017

Self, S. (2006). The effects and consequences of very large explosive volcanic eruptions. *Philosophical Transactions of the Royal Society A: Mathematical Physical and Engineering Sciences*, *364*(1845), 2073–2097. https://doi.org/10.1098/rsta.2006.1814

Self, S., Gertisser, R., Thordarson, T., Rampino, M. R., & Wolff, J. A. (2004). Magma volume, volatile emissions, and stratospheric aerosols from the 1815 eruption of Tambora. *Geophysical Research Letters*, *31*, L20608. https://doi.org/10.1029/2004GL020925

Sigmarsson, O., Laporte, D., Carpentier, M., Devouard, B., Devidal, J.-L., & Marti, J. (2013). Formation of U-depleted rhyolite from a basanite at El Hierro, Canary Islands. *Contributions to Mineralogy and Petrology*, *165*(3), 601–622. https://doi.org/10.1007/s00410-012-0826-5

Signorelli, S., & Carroll, M. R. (2002). Experimental study of Cl solubility in hydrous alkaline melts: Constraints on the theoretical maximum amount of Cl in trachytic and phonolitic melts. *Contributions to Mineralogy and Petrology*, *143*(2), 209–218. https://doi.org/10.1007/s00410-001-0320-y

Sigurdsson, H. (1972). Partly-welded pyroclast flow deposits in Dominica, Lesser Antilles. *Bulletin Volcanologique*, *36*(1), 148–163. https://doi.org/10.1007/BF02596987

Smith, A. L., Roobol, M. J., Mattioli, G. S., Fryxell, J. E., Daly, G. E., & Fernandez, L. A. (2013). *The volcanic geology of the mid-arc Island of Dominica* (Vol. 496). Geological Society of America.

Sobolev, A. V. (1996). Melt inclusions in minerals as a source of principle petrological information. *Journal of Petrology*, *4*(3), 228–239.

Sobolev, A. V., & Danyushevsky, L. V. (1994). Petrology and geochemistry of boninites from the north termination of the Tonga Trench: Constraints on the generation conditions of primary high-Ca boninite magmas. *Journal of Petrology*, *35*(5), 1183–1211. https://doi.org/10.1093/petrology/35.5.1183

Solaro, C., Martel, C., Champallier, R., Boudon, G., Balcone-Boissard, H., & Pichavant, M. (2019). Petrological and experimental constraints on magma storage for large pumiceous eruptions in Dominica island (Lesser Antilles). *Bulletin of Volcanology*, *81*(9), 1–22. https://doi.org/10.1007/s00445-019-1313-x

Sparks, R. S. J., & Cashman, K. V. (2017). Dynamic magma systems: Implications for forecasting volcanic activity. *Elements*, *13*(1), 35–40. https://doi.org/10.2113/gselements.13.1.35

Sparks, R. S. J., Sigurdsson, H., & Carey, S. N. (1980). The entrance of pyroclastic flows into the sea I. Oceanographic and geologic evidence from Dominica, Lesser Antilles. *Journal of Volcanology and Geothermal Research*, *7*(1), 87–96. https://doi.org/10.1016/0377-0273(80)90021-9

Vidal, C. M., Métrich, N., Komorowski, J.-C., Pratomo, I., Michel, A., Kartadinata, N., et al. (2016). The 1257 Samalas eruption (Lombok, Indonesia): The single greatest stratospheric gas release of the Common Era. *Scientific Reports*, *6*(1), 1–13. https://doi.org/10.1038/srep34868

Wadge, G. (1984). Comparison of volcanic production rates and subduction rates in the Lesser Antilles and Central America. *Geology*, *12*(9), 555. https://doi.org/10.1130/0091-7613(1984)12<555:COVPRA>2.0.CO;2

Wadge, G., Herd, R., Ryan, G., Calder, E. S., & Komorowski, J.-C. (2010). Lava production at Soufrière Hills Volcano, Montserrat: 1995–2009: LAVA production at Montserrat. *Geophysical Research Letters*, *37*, L00E03. https://doi.org/10.1029/2009GL041466

Wallace, P. J. (2005). Volatiles in subduction zone magmas: Concentrations and fluxes based on melt inclusion and volcanic gas data. *Journal of Volcanology and Geothermal Research*, *140*(1), 217–240. https://doi.org/10.1016/j.jvolgeores.2004.07.023

Wallace, P. J., Plank, T., Edmonds, M., & Hauri, E. H. (2015). Volatiles in magmas. In *The encyclopedia of volcanoes* (pp. 163–183). Academic Press. https://doi.org/10.1016/B978-0-12-385938-9.00007-9

Watts, R. B., Robertson, R. E., Abraham, W., Cole, P., de Roche, T., Edwards, S., et al. (2012). *Elevated seismic activity beneath the slumbering Morne aux Diables Volcano, northern Dominica and the monitoring role of the seismic research centre* (Vol. 53, pp. V53E–V2879E). AGU Fall Meeting Abstracts.

Webster, J. D. (1997). Chloride solubility in felsic melts and the role of chloride in magmatic degassing. *Journal of Petrology*, *38*(12), 1793–1807. https://doi.org/10.1093/petroj/38.12.1793

Whitham, A. G. (1989). The behaviour of subaerially produced pyroclastic flows in a subaqueous environment: Evidence from the Roseau eruption, Dominica, West Indies. *Marine Geology*, *86*(1), 27–40. https://doi.org/10.1016/0025-3227(89)90016-9